Microfluidics and Nanofluidics (2021) 25:31
https://doi.org/10.1007/s10404-021-02426-x

RESEARCH PAPER

Design and application of a self-pumping microfluidic staggered herringbone mixer

Robert B. Channon[1] · Ruth F. Menger[2] · Wei Wang[3] · Daniel B. Carrão[4] · Sravanthi Vallabhuneni[5] · Arun K. Kota[5] · Charles S. Henry[1,6,7]

Received: 19 November 2020 / Accepted: 23 January 2021

Abstract

The rapid mixing of reagents is critical to a wide range of chemical and biological reactions but is difficult to implement in microfluidic devices, particularly in capillary action/passive pumping devices or in point-of-need environments. Here, we develop a self-pumping asymmetric staggered herringbone mixer made from only laser-ablated glass and tape. This lab-on-a-chip platform is capable of rapid flow (0.14 mL min^{-1}, 1 cm s^{-1}) and fast mixing (< 10 s) without external forces or pumps and is amenable to the flow of non-aqueous solvents. Furthermore, the degree of mixing and flow rates are easily tunable through the length and depth of the herringbone grooves, and the thickness of the double-sided tape that defines the channel height, respectively. The device utility is demonstrated for chemical and biological assays through the reaction of Ni(II) and DMG in ethanol/water and the enzymatic reaction of o-dianisidine with peroxidase, respectively.

Keywords Microfluidics · Herringbone · Micromixer · Lab-on-a-chip · Kinetics · Passive flow

1 Introduction

Microfluidic and lab-on-a-chip devices are transformative tools for carrying out chemical and biological reactions across a wide range of disciplines, from drug discovery to biomarker monitoring (Nahavandi et al. 2014; Regnault et al. 2018). These applications are driven by the small sample volume requirements, high device portability, and inexpensive setup and reaction costs compared to conventional approaches. Three key current challenges in the microfluidics/lab-on-a-chip community are (1) generating fluid flow cheaply and easily in point-of-care environments, (2) the ability to transport non-aqueous solvents, and (3) the fast and complete mixing of reagents (Cai et al. 2017; Chin et al. 2012; Renckens et al. 2011).

The most common approach to generate fluid flow in microfluidic devices is through syringe pumps, but these are unsuitable for point-of-care flow generation due to the bulky size and requirement of electricity. Portable plug-and-play pumps or valves have been designed to overcome this challenge, though they are often application-specific (e.g., fixed flow rates) (Feeny et al. 2016; Park and Park, 2019; Zhang et al. 2020). Capillary action-based flow is also used with hydrophilic materials such as paper or glass, although the flow rates can be slow and integration of complex designs

Robert B. Channon, Ruth F. Menger and Wei Wang contributed equally to this work.

✉ Arun K. Kota
akota2@ncsu.edu

✉ Charles S. Henry
chuck.henry@colostate.edu

1 Department of Bioengineering, Imperial College London, London W12 0BZ, UK

2 Department of Chemistry, Colorado State University, Fort Collins, CO 80523, USA

3 Department of Mechanical, Aerospace and Biomedical Engineering, University of Tennessee, Knoxville, TN 37996, USA

4 Departamento de Química, Faculdade de Filosofia, Ciências e Letras de Ribeirão Preto, Universidade de São Paulo, Ribeirão Preto, SP 14090-901, Brazil

5 Department of Mechanical and Aerospace Engineering, North Carolina State University, Raleigh, NC 27695, USA

6 Department of Chemical and Biological Engineering, Colorado State University, Fort Collins, CO 80523, USA

7 School of Biomedical Engineering, Colorado State University, Fort Collins, CO 80523, USA

Published online: 19 March 2021

(e.g., mixing and sensing modules) can be challenging (Carrell et al. 2019; Iliescu et al. 2012).

Many microfluidic devices are made of materials (like polydimethylsiloxane and paper) that are incompatible with non-aqueous solvents. This limits the scope of microfluidic devices (Channon et al. 2016). Cyclic olefin copolymers and hybrid materials such as fluorinated polymers coated onto PDMS can accommodate non-aqueous solvents, but the preparation of these materials is often more complex and expensive (Illa et al. 2010; Renckens et al. 2011). Paper-based devices are ideally suited for point-of-care environments, however, the flow rates are generally slow and the inks used to define channels are not stable in non-aqueous solvents (Cardoso et al. 2017; Park et al. 2016).

Micromixers are critical components to conduct chemical or biological reactions and/or to sense analytes in microfluidic or lab-on-a-chip devices (Jeong et al. 2010). Micromixers can be divided into active and passive mixers. Active micromixers employ an external stimulus to mix fluids, including magnetic beads, temperature, pressure, acoustics, digital droplets, or an electric field (Bayareh et al. 2020; Lynn et al. 2008; Shanko et al. 2019; Srinivasan et al. 2004; Ward and Fan, 2015). Active mixers typically provide a high degree of mixing and are especially useful for systems with low Reynolds numbers ($Re < 1$) to overcome low flow rates and high viscosity, but these mixers are unsuitable for point-of-care devices due to the added cost and increased size that comes with the integration of an external power source to a microfluidic device (Capretto et al. 2011). Passive micromixers rely on shrewd device designs to enhance advective and diffusive mixing without external forces, for example, serpentines, splitting then recombination of streams, multiphase flow, and integration of obstacles, grooves, or ridges (Bayareh et al. 2020; Chen et al. 2018; Feng et al. 2019; Seong and Crooks 2002; Shanko et al. 2019; Wang et al. 2019a; Ward and Fan 2015). Compared to active mixers, passive micromixers typically require longer channel lengths and longer mixing times to achieve complete mixing. Furthermore, there are very few effective passive micromixers for capillary-based flow systems (Gervais et al. 2011; Glavan et al. 2013; Lillehoj et al. 2010; Taher et al. 2017).

Among passive mixers, herringbone mixers are particularly popular due to the efficient mixing over short channel lengths. Herringbone devices feature an array of grooves in the wall of a microfluidic channel (Stroock et al. 2002). Fluid enters these grooves and recirculates into the main channel, generating complex circulating flows that result in fluid mixing. The speed and extent of mixing are controlled by the length of the herringbone, the channel dimensions, and the flow rate (Williams et al. 2008). Patterning herringbones into both the top and bottom channel walls has been shown to improve the mixing efficiency, although this is difficult to implement depending on the fabrication procedure and device materials (Choudhary et al. 2011; Feng et al. 2019; Hossain et al. 2011). Herringbone micromixers have been employed for micromixing in a range of applications (Liu et al. 2014; Wang et al. 2016), but rarely in point-of-care environments.

In this work, we demonstrate for the first time an asymmetric two-faced staggered herringbone passive micromixer combined with a passive/capillary action flow device. Our design is based on a self-pumping device made from glass and tape which is simple, inexpensive, and fast to manufacture. This novel fabrication approach provides fast flow rates and rapid mixing that have not been achieved previously in other passive flow herringbone devices. To demonstrate the scope of this point-of-care device, we investigate the application of the microfluidic device with two kinetically fast chemical and biological reactions.

2 Materials and methods

2.1 Fabrication and operation of herringbone device

Microfluidic devices with herringbone grooves were fabricated via a simple cutting and stacking method. Three sets of herringbone grooves were rastered onto each glass slide (Glass D, Nexterion) with a laser cutter (Epilog Zing), operated at a resolution of 500 dpi, 100% laser power, and 25% scanning speed. Each of the 3 sets of herringbones consisted of 15 herringbone grooves with a width of ~ 285–300 µm, depth of ~ 120 µm, and inter-groove spacing of ~ 530 µm (i.e., valley to valley), which was achieved through 8 laser engraving scans (Fig. S1). The angle between the long and short grooves is 105.7°. The channel height, herringbone groove depth were optimized to provide the most efficient mixing (Hossain et al. 2011; Williams et al. 2008). After fabrication, the glass slides were cleaned by ultrasonication in acetone for 10 min, rinsed with DI water, and dried with nitrogen.

To join the glass slides and define the channel height and width, double-sided tape (3M Scotch) was carefully cut with a laser ablator and aligned on the glass slide to form a ~ 3 mm wide Y-shaped channel (~ 50 µm channel height) over the herringbone structures (Fig. S2). A template was used to ensure proper alignment. Another glass slide with herringbone structures was placed on the tape layer and firmly pressed to form the microfluidic device. An asymmetric design was employed where the herringbone grooves in the top face of the channel were oriented in an offset pattern to the bottom face to enhance the mixing (Fig. 1a) (Choudhary et al. 2011; Hossain et al. 2011). A coating of 3M instant adhesive (SF 100) was applied to the sidewall with the channel inlets to prevent the undesired spreading of

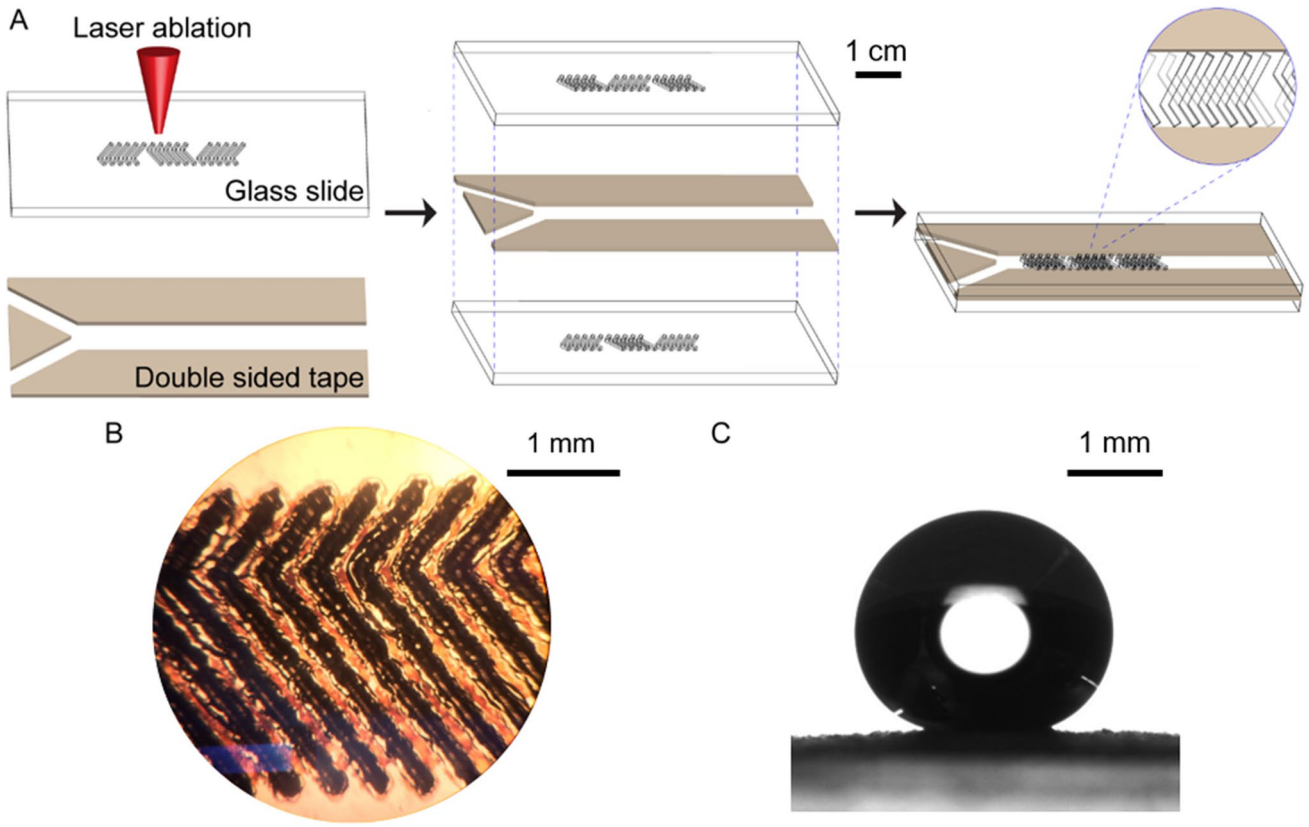

Fig. 1 **a** Schematic of device fabrication, **b** Microscope image of lasered grooves, **c** 10 µL droplet of water on superomniphobic paper (contact angle 165°)

liquid droplets upon contacting the device entrance. Prior to experiments, the device was cleaned by flushing with ethanol, then water, and dried thoroughly with nitrogen.

To demonstrate the rapid mixing of our self-pumping microfluidic devices, Liquid droplets containing reagents were placed on a piece of superomniphobic paper, which displays extreme repellence to liquids with a wide range of surface tension (Movafaghi et al. 2019; Vahabi et al. 2017, 2018; Wang et al. 2019c). The droplets were spaced accordingly to line up with the entrance of the microfluidic device. The device was moved toward the droplets until contact with the glass initiated fluid flow into the channel. The experiments were recorded with a digital camera (Canon) and then analyzed using NIH ImageJ software as described in the ESI.

2.2 Fabrication of superomniphobic paper

Superomniphobic paper was fabricated through liquid phase silanization of Whatman filter paper 8, as previously described (Channon et al. 2019; Wang et al. 2019b). The filter paper was exposed to oxygen plasma for 10 min and then immersed in a mixture of 20 mL hexane and 600 µL of heptadecafluoro-1,1,2,2-tetrahydrodecyltrichlorosilane (FDTS) for 3 days at room temperature. The paper was then washed with hexane and dried with nitrogen.

2.3 Ni-DMG reaction

The colorimetric reaction of nickel with dimethylglyoxime (DMG) was used as a representative inorganic reaction (Fig. S3). A solution of 2.25 mM nickel (nickel (II) sulfate hexahydrate, Sigma Aldrich) was prepared in 1:1 mix of ethanol and pH 5 acetate buffer. A solution of 4.5 mM DMG (Fluka) was prepared in 50% v/v ethanol: DI water. 50 µL droplets of each reagent were mixed in the device.

2.4 HRP-H_2O_2 reaction

The enzymatic turnover of H_2O_2 by horseradish peroxidase was used as a representative biological reaction to evaluate enzyme kinetics using the herringbone device (Fig. S4). Ten solutions of H_2O_2 (Sigma Aldrich) were prepared in DI water between 0.001 mM and 0.06 mM (0.005–0.2% v/v). A 0.018 M solution of o-dianisidine dihydrochloride (Sigma Aldrich) in DI water was used for all experiments. A 32.5 U mL^{-1} solution of horseradish peroxidase (HRP, Sigma Aldrich, peroxidase from horseradish Type VI, > 250

U mg^{-1}) was prepared in DI water immediately prior to use. All solutions were prepared in DI water instead of buffer due to the higher o-dianisidine (OD) solubility in DI water. In the device, a 30 µL droplet of a 50:50 mixture of OD and HRP was mixed with a 30 µL droplet of H_2O_2. Videos were recorded for each reaction and analyzed in ImageJ (ESI).

3 Results and discussion

Given the challenges associated with mixing in passive flow devices, we sought to determine if we could use herringbone-based mixing devices to achieve mixing in a capillary flow device. Our device design (Fig. 1a) was adapted from that used in multilayered paper-based microfluidic devices without mixers as well as the literature on staggered one- and two-faced herringbone microfluidic mixers (Channon et al. 2019; Choudhary et al. 2011; Lin et al. 2013; Stroock et al. 2002). The device itself is fabricated using a laser cutter to etch the herringbone grooves into glass slides and sealing with double-sided adhesive to form the microfluidic channel. The device design, dimensions, and characterization by optical profilometry are provided in the ESI (Fig. S1 and S2). The number and depth of the herringbone sets, as well as the height of the tape, were previously optimized and chosen for both efficient mixing and consistency of the device (Hossain et al. 2011; Williams et al. 2008). The staggered herringbone grooves in the top and bottom faces of the channel were offset yielding an asymmetric pattern. This provides enhanced mixing over herringbones in a single face or symmetric herringbones in two faces, and likely results in four circular flows across the channel cross-section as previously described (Choudhary et al. 2011). To establish fluid flow, reactants were placed as droplets on superomniphobic paper (contact angle ≈ 165° for ~ 10 µL, Fig. 1c), which displays extreme repellence to liquids with a wide range of surface tension (Movafaghi et al. 2019; Vahabi et al. 2017, 2018; Wang et al. 2019c). Moving the device toward the droplets until contact with the glass initiates fast fluid flow (0.14 mL min^{-1}, 1 cm s^{-1}) of the reactants into the channel due to capillarity.

To illustrate the enhanced mixing in the herringbone device, aqueous droplets of blue and yellow food dyes were mixed forming a green color. The pixel count for each color was measured in ImageJ before and after the herringbones (Fig. S3). Three device configurations were evaluated: a control device with no herringbone grooves, a device with one slide with ablated herringbone grooves, and one with two slides with herringbone grooves in an asymmetric pattern (Fig. 2, ESI videos 'BY dye control', 'BY dye 1 side herringbone', and 'BY dye 2 sides herringbone'). In the absence of herringbone grooves, mixing only occurred at the interface of the two colors (20% green pixels). The Reynolds (Re) and Peclet (Pe) numbers for our system are 0.98 and 490, respectively. This suggests flow in the devices is laminar, and mass transport is likely mixed diffusive and convective. In fact, in the control device without herringbones, an 8 m long channel would be required to fully mix the two colors (Stroock et al. 2002). Partial mixing was achieved when one channel wall contained herringbone grooves (52% green pixels), but for complete mixing in the length of the herringbone grooves (3.3 cm), two faces with herringbone grooves were required (100% green pixels). This result is in line with previous studies on improved mixing efficiencies with multiple walls of herringbone grooves compared to a single set (Choudhary et al. 2011; Hossain et al. 2011). As the three sets of herringbones deliver complete mixing, we anticipate most solvents and solvent mixtures would also mix satisfactorily through the current design. The fabrication method is designed as such to be able to tune the device to the application (i.e., choice of tape to define the channel height or number of herringbones). The speed and degree of mixing can be tuned with these parameters depending on the miscibility and viscosity of the reagents and the application.

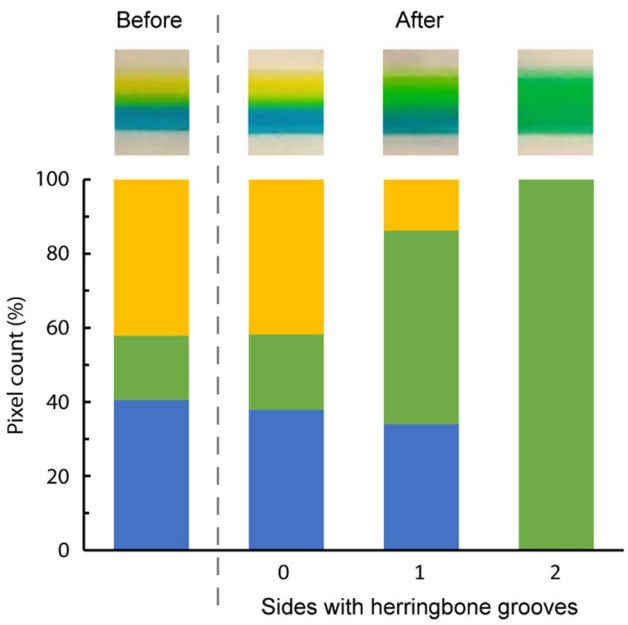

Fig. 2 Analysis of mixing blue and yellow dyes to form a green color with 0, 1, and 2 slides with herringbone grooves. Images (top row) were taken just before and just after the herringbones (colour figure online)

Manufacturing microfluidic devices with herringbone grooves in the top and bottom channel walls is challenging using traditional micromachining methods. Typically, microfluidic devices are made with a channel in one material, like PDMS, which is bonded to a base substrate, like a glass coverslip, using plasma treatment. It can be challenging to make herringbone grooves in PDMS since these devices

typically require photolithography as a fabrication process (Stroock et al. 2002; Williams et al. 2008). Our proposed device is made of two glass slides bonded with double-sided adhesive. The herringbone grooves are etched into each slide with a laser cutter, and the channel height and width are controlled by the placement and height of double-sided adhesive. Our device features a channel width of 3 mm and height of 50 µm, representing a hydraulic diameter of 98 µm. The use of wide channels with small heights is fairly common in microfluidic devices, e.g. in channel flow cells with electrochemical sensing (Channon et al. 2015). In addition, the flow and mixing of small sample volumes (ca. 40 µL) fit the definition of a microfluidic device. Given the benefits of the fabrication method (fast, easy, inexpensive), we envision these glass/tape herringbone devices as disposable mixers for point-of-care applications.

As proof of concept to demonstrate the device scope, two representative chemical and biological application reactions were chosen. First, the detection of Ni(II) in the environment, which is important due to the environmental abundance of Ni(II) and potential health issues such as reduced lung function and cancer (Denkhaus and Salnikow, 2002). A common colorimetric assay for Ni(II) detection is the reaction with dimethylglyoxime (DMG) in ethanol:H_2O (Fig. S4) (Cate et al. 2015; Mentele et al. 2012). This reaction produces a reddish-pink precipitate which is insoluble in water, as shown in Fig. 3b (ESI video 'Ni-DMG herringbone'). Note, in the absence of the herringbones, no precipitate is observed (Fig. 3a, ESI video 'Ni-DMG control'). Since the DMG is dissolved in ethanol, the Ni-DMG reaction also demonstrates that the device applicability for reactions in non-aqueous solvents, which are commonplace in the industry. Many microfluidic materials (polydimethylsiloxane, PDMS, paper) are limited by incompatibility with non-aqueous solvents (Channon et al. 2016), but with the herringbone device being made out of glass, it is compatible with organic solvents as there were no visible adverse effects like degradation or delamination.

The mixing device can also be used for biological assays such as the enzymatic reaction of hydrogen peroxide (H_2O_2) and horseradish peroxidase (HRP), using o-dianisidine (OD) as a colorimetric indicator (Fig. S5). The reaction of HRP with H_2O_2 is important for many bioassays where HRP is a label (Hempen and Karst 2006). H_2O_2 is turned over by the HRP, oxidizing the OD which turns from colorless to dark brown (Fig. 4a, ESI video 'HRP herringbone'). Without the herringbone grooves, mixing only occurs at the interface of the two liquids due to diffusion (Fig. 4B, ESI video

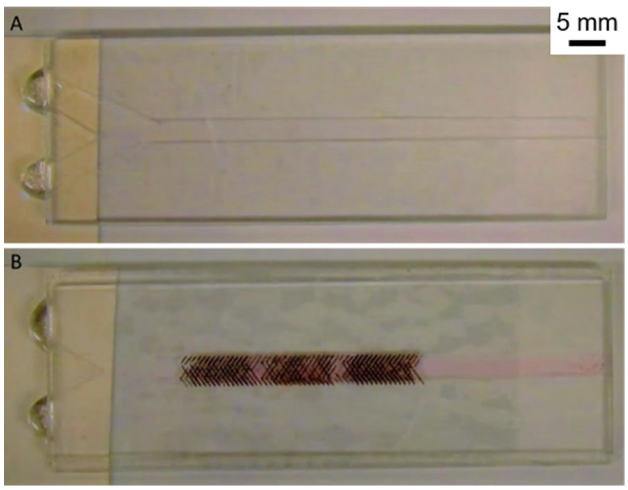

Fig. 3 Nickel (top droplet) mixing with DMG (bottom droplet) in a device without herringbone grooves (**a**) and with herringbone grooves (**b**)

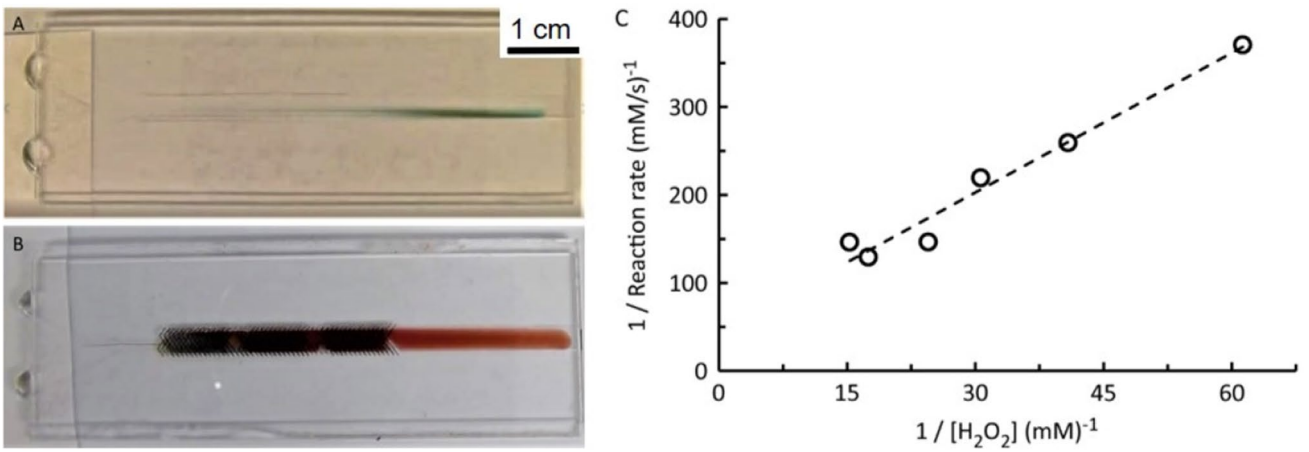

Fig. 4 Reaction of hydrogen peroxide (top droplets) with o-dianisidine and horseradish peroxidase (bottom droplet) in a device without herringbone grooves (**a**) and with herringbone grooves (**b**). The reagents are fully mixed in B to produce brown o-dianisidine. **c** Lineweaver–Burk plot of the enzymatic turnover of hydrogen peroxide

'HRP control'). To demonstrate that the herringbone device gives similar results to traditional microfluidic devices and bulk solution reactions, Michaelis–Menten kinetics were determined for this reaction using the micromixing device (details in the ESI, Fig. S6, S7). In short, videos with various concentrations of H_2O_2 were analyzed and the brown color intensity was measured in ImageJ over the course of each video. This yielded the reaction rate, and its inverse was plotted against the inverse of H_2O_2 concentration, generating a Lineweaver–Burk plot (Fig. 4c) (Boehle et al. 2018). Values for K_m and k_{cat} were determined to be 0.119 mM and 7.61 s^{-1}, respectively, and are comparable to those found in the literature (Ugarova et al. 1981). The similarity in measured values indicates the viability of this simple mixing system for carrying out kinetic reactions. In addition, the herringbone device could easily be used for other biological applications, for example, investigating the binding kinetics between fluorescently tagged antibodies and antigens without needing surface plasmon resonance measurements (Lago et al. 2018).

Previous herringbone devices have been fabricated using standard photolithography methods and a SU-8 photoresist, forming the channel when PDMS is plasma-bonded to a glass slip (Stroock et al. 2002; Williams et al. 2008). This method is time-intensive and expensive in comparison to the described approach of laser ablating the glass slides and sealing with tape. Each device costs ~ $0.40 and takes ~ 7 min to make by hand. Since the design is printed from a CAD file, changing the design to prototype new devices is fast and simple in comparison to making a new photoresist mold. Glass also has high solvent stability compared to other common materials used to make microfluidic devices. For example, PDMS swells in nonpolar solvents such as hydrocarbons, toluene, and dichloromethane (Lee et al. 2003), resulting in deformed channels and altered dimensions, which changes the fluid velocity and mixing capacity as well as affecting any sensing elements. Typically, paper-based devices use wax to form hydrophobic channels on the paper (Altundemir et al. 2017). Wax is not compatible with organic solvents, leaving the device without any barriers to direct fluid flow. Conversely, glass is compatible with a wider range of solvents (Lee et al. 2003), allowing this herringbone device to be used for a variety of reactions without compromising the integrity of the device.

4 Conclusion

A new herringbone microfluidic mixer is presented that can achieve complete mixing of small volumes over short times and distances. Crucially, these devices employ passive pumping (capillary action) and are capable of transporting both aqueous and organic solvents which are typically challenging to use in self-pumping devices. Laser cutting the asymmetric staggered herringbone grooves into glass slides as the channel walls delivers a fast, simple, inexpensive, and easily modifiable fabrication that has not been previously demonstrated as well as achieving fast flow rates and rapid mixing. The flow rate can easily be changed by altering the channel height through the choice of double-sided tape thickness or the number of tape layers (commercially available tapes range from 50 to 230 μm thicknesses) (Channon et al. 2019). The degree of mixing can be simply altered through the number of herringbone grooves, or the depth of the grooves (through the number of lasering rasters) (Choudhary et al. 2011; Hossain et al. 2011; Stroock and McGraw 2004; Williams et al. 2008). The device can be used for a range of biological and environmental applications, including inorganic, organic, and enzymatic reactions. Furthermore, relevant data like enzyme kinetics can be easily deduced from the device through colorimetric image analysis and our devices are amenable to other microfluidic sensing formats e.g., fluorescence and electrochemical detection. This device has great potential as a disposable mixer for point-of-care applications. Future work will seek to expand the application of these devices to a wider range of reactions in non-aqueous solvents, as well as to conduct finite element modeling of the device to understand the mixing in a capillary flow-driven asymmetric staggered herringbone mixer and optimize the device design (Choudhary et al. 2011; Hama et al. 2018; Hossain et al. 2010).

Supplementary Information The online version contains supplementary material available at https://doi.org/10.1007/s10404-021-02426-x.

Acknowledgements A.K.K. acknowledges financial support under award 1751628 from the National Science Foundation and under awards R01HL135505 and R21HL139208 from the National Institutes of Health. C.S.H. acknowledges support under R33ES024719. Additional support was provided by Colorado State University.

Compliance with ethical standards

Conflict of interest The authors have no conflicts to declare.

References

Altundemir S, Uguz A, Ulgen K (2017) A review on wax printed microfluidic paper-based devices for international health. Biomicrofluidics 11:041501

Bayareh M, Ashani MN, Usefian A (2020) Active and passive micromixers: a comprehensive review. Chem Eng Process 147:107771

Boehle KE, Doan E, Henry S, Beveridge JR, Pallickara SL, Henry CS (2018) Single board computing system for automated colorimetric analysis on low-cost analytical devices. Anal Methods 10:5282–5290

Cai G, Xue L, Zhang H, Lin J, Cai G, Xue L, Zhang H, Lin J (2017) A review on micromixers. Micromachines 8:274–274

Capretto L, Cheng W, Hill M and Zhang X (2011) Microfluidics. In: Lin, B. (ed), Springer Berlin Heidelberg, Berlin, Heidelberg, pp. 27–68.

Cardoso TMG, De Souza FR, Garcia PT, Rabelo D, Henry CS, Coltro WKT (2017) Versatile fabrication of paper-based microfluidic devices with high chemical resistance using scholar glue and magnetic masks. Anal Chim Acta 974:63–68

Carrell C, Kava A, Nguyen M, Menger RF, Munshi Z, Call Z, Nussbaum M, Henry C (2019) Beyond the lateral flow assay: a review of paper-based microfluidics. Microelectron Eng 206:45–54

Cate DM, Noblitt SD, Volckens J, Henry CS (2015) Multiplexed paper analytical device for quantification of metals using distance-based detection. Lab Chip 15:2808–2818

Channon RB, Joseph MB, Bitziou E, Bristow AWT, Ray AD, Macpherson JV (2015) Electrochemical flow injection analysis of hydrazine in an excess of an active pharmaceutical ingredient: achieving pharmaceutical detection limits electrochemically. Anal Chem 87:10064–10071

Channon RB, Joseph MB, Macpherson JV (2016) Additive manufacturing for electrochemical (micro)fluidic platforms. Electrochem Soc Interface 25:63–68

Channon RB, Nguyen MP, Henry CS, Dandy DS (2019) Multilayered microfluidic paper-based devices: characterization, modeling, and perspectives. Anal Chem 91:8966–8972

Chen C, Zhao Y, Wang J, Zhu P, Tian Y, Xu M, Wang L, Huang X (2018) Passive Mixing inside. Microdroplets Micromachines 9:160

Chin CD, Linder V, Sia SK (2012) Commercialization of microfluidic point-of-care diagnostic devices. Lab Chip 12:2118

Choudhary R, Bhakat T, Kumar Singh R, Ghubade A, Mandal S, Ghosh A, Rammohan A, Sharma A, Bhattacharya S (2011) Bilayer staggered herringbone micro-mixers with symmetric and asymmetric geometries. Microfluid Nanofluid 10:271–286

Denkhaus E, Salnikow K (2002) Nickel essentiality, toxicity, and carcinogenicity. Crit Rev Oncol Hemat 42:35–56

Feeny RM, Puissant NL, Henry CS (2016) Degassed PDMS pump for controlled extraction from dried filter samples in microfluidic devices. Anal Methods 8:8243–8370

Feng X, Ren Y, Hou L, Tao Y, Jiang T, Li W, Jiang H (2019) Tri-fluid mixing in a microchannel for nanoparticle synthesis. Lab Chip 19:2936–2946

Gervais L, Hitzbleck M, Delamarche E (2011) Capillary-driven multiparametric microfluidic chips for one-step immunoassays. Biosens Bioelectron 27:64–70

Glavan AC, Martinez RV, Maxwell EJ, Subramaniam AB, Nunes RMD, Soh S, Whitesides GM (2013) Rapid fabrication of pressure-driven open-channel microfluidic devices in omniphobic RF paper. Lab Chip 13:2922

Hama B, Mahajan G, Fodor PS, Kaufman M, Kothapalli CR (2018) Evolution of mixing in a microfluidic reverse-staggered herringbone micromixer. Microfluid Nanofluid 22:1–14

Hempen C, Karst U (2006) Labeling strategies for bioassays. Anal Bioanal Chem 384:572–583

Hossain S, Husain A, Kim K-Y (2010) Shape optimization of a micromixer with staggered-herringbone grooves patterned on opposite walls. Chem Eng J 162:730–737

Hossain S, Husain A, Kim KY (2011) Optimization of micromixer with staggered herringbone grooves on top and bottom walls. Eng Appl Comp Fluid Mech 5:506–516

Iliescu C, Taylor H, Avram M, Miao J, Franssila S (2012) A practical guide for the fabrication of microfluidic devices using glass and silicon. Biomicrofluidics 6:016505

Illa X, Ordeig O, Snakenborg D, Romano-Rodríguez A, Compton RG, Kutter JP (2010) A cyclo olefin polymer microfluidic chip with integrated gold microelectrodes for aqueous and non-aqueous electrochemistry. Lab Chip 10:1254

Jeong GS, Chung S, Kim C-B, Lee S-H (2010) Applications of micromixing technology. Analyst 135:460

Lago S, Nadai M, Rossetto M, Richter SN (2018) Surface plasmon resonance kinetic analysis of the interaction between G-quadruplex nucleic acids and an anti-G-quadruplex monoclonal antibody. Biochim Biophys Act Gen Subj 1862:1276–1282

Lee JN, Park C, Whitesides GM (2003) Solvent compatibility of Poly(dimethylsiloxane)-based microfluidic devices. Anal Chem 75:6544–6554

Lillehoj PB, Wei F, Ho C-M (2010) A self-pumping lab-on-a-chip for rapid detection of botulinum toxin. Lab Chip 10:2265

Lin D, He F, Liao Y, Lin J, Liu C, Song J, Cheng Y (2013) Three-dimensional staggered herringbone mixer fabricated by femtosecond laser direct writing. J Opt 15:025601–025601

Liu B, Wu T, Yang X, Wang Z, Du Y (2014) Portable microfluidic chip based surface-enhanced raman spectroscopy sensor for crystal violet. Anal Lett 47:2682–2690

Lynn NS, Henry CS, Dandy DS (2008) Microfluidic mixing via transverse electrokinetic effects in a planar microchannel. Microfluid Nanofluid 5:493–505

Mentele MM, Cunningham J, Koehler K, Volckens J, Henry CS (2012) Microfluidic paper-based analytical device for particulate metals. Anal Chem 84:4474–4480

Movafaghi S, Cackovic MD, Wang W, Vahabi H, Pendurthi A, Henry CS, Kota AK (2019) Superomniphobic papers for on-paper pH sensors. Adv Mater Interfaces 6:1900232

Nahavandi S, Baratchi S, Soffe R, Tang S-Y, Nahavandi S, Mitchell A, Khoshmanesh K (2014) Microfluidic platforms for biomarker analysis. Lab Chip 14:1496–1514

Park J, Park J-K (2019) Integrated microfluidic pumps and valves operated by finger actuation. Lab Chip 19:5

Park SH, Maruniak A, Kim J, Yi G-R, Lim SH (2016) Disposable microfluidic sensor arrays for discrimination of antioxidants. Talanta 153:163–169

Regnault C, Dheeman D, Hochstetter A (2018) Microfluidic Devices for Drug Assays. High-Throughput 7:18

Renckens TJA, Janeliunas D, Van Vliet H, Van Esch JH, Mul G, Kreutzer MT (2011) Micromolding of solvent resistant microfluidic devices. Lab Chip 11:2035

Seong GH, Crooks RM (2002) Efficient mixing and reactions within microfluidic channels using microbead-supported catalysts. J Am Chem Soc 124:13360–13361

Shanko E-S, Van De Burgt Y, Anderson PD, Den Toonder JMJ (2019) Microfluidic magnetic mixing at low reynolds numbers and in stagnant fluids. Micromachines 10:731

Srinivasan V, Pamula VK, Fair RB (2004) An integrated digital microfluidic lab-on-a-chip for clinical diagnostics on human physiological fluids. Lab Chip 4:310–315

Stroock AD, McGraw GJ (2004) Investigation of the staggered herringbone mixer with a simple analytical model. Phil Trans R Soc Lond A 362:971–986

Stroock AD, Dertinger SKW, Ajdari A, Mezic I, Stone HA, Whitesides GM (2002) Chaotic mixer for microchannels. Science 295:647–651

Taher AJ, Benjamin FP, Lagae L (2017) A valveless capillary mixing system using a novel approach for passive flow control. Microfluid Nanofluid 21:10

Ugarova NN, Lebedeva OV, Berezin IV (1981) Horseradish peroxidase catalysis I. Steady-state kinetics of peroxidase-catalyzed individual and co-oxidation of potassium ferrocyanide and o-dianisidine by hydrogen peroxide. J Mol Catal 13:215–225

Vahabi H, Wang W, Davies S, Mabry JM, Kota AK (2017) Coalescence-induced self-propulsion of droplets on superomniphobic surfaces. ACS Appl Mater 9:29328–29336

Vahabi H, Wang W, Mabry JM, Kota AK (2018) Coalescence-induced jumping of droplets on superomniphobic surfaces with macrotexture. Sci Adv 4:3488

Wang S, Thomas A, Lee E, Yang S, Cheng X, Liu Y (2016) Highly efficient and selective isolation of rare tumor cells using a microfluidic chip with wavy-herringbone micro-patterned surfaces. Analyst 141:2228–2237

Wang J, Zhang N, Chen J, Rodgers VGJ, Brisk P, Grover WH (2019a) Finding the optimal design of a passive microfluidic mixer. Lab Chip 19:3618–3627

Wang W, Du X, Vahabi H, Zhao S, Yin Y, Kota AK, Tong T (2019b) Trade-off in membrane distillation with monolithic omniphobic membranes. Nat Comm 10:1–9

Wang W, Vahabi H, Movafaghi S, Kota AK (2019c) Superomniphobic surfaces with improved mechanical durability: synergy of hierarchical texture and mechanical interlocking. Adv Mater Interfaces 6:1900538

Ward K, Fan ZH (2015) Mixing in microfluidic devices and enhancement methods. J Micromech Microeng 25:094001

Williams MS, Longmuir KJ, Paul Y (2008) A practice guide to the staggered herringbone mixer. Lab Chip 8:1121–1129

Zhang X, Xia K, Ji A (2020) A portable plug-and-play syringe pump using passive valves for microfluidic applications. Sens Actuators B Chem 304:127331